^{18}F-FPPRGD2 and ^{18}F-FDG PET of Response to Abraxane Therapy

Xilin Sun[1,2], Yongjun Yan[1], Shuanglong Liu[3], Qizhen Cao[3], Min Yang[1], Nouri Neamati[4], Baozhong Shen[2], Gang Niu[1,5], and Xiaoyuan Chen[1]

[1]Laboratory of Molecular Imaging and Nanomedicine, National Institute of Biomedical Imaging and Bioengineering, National Institutes of Health, Bethesda, Maryland; [2]Department of Medical Imaging and Nuclear Medicine, the 4th Affiliated Hospital, Harbin Medical University, Harbin, China; [3]Molecular Imaging Program at Stanford (MIPS), Department of Radiology, Stanford University School of Medicine, Stanford, California; [4]School of Pharmacy, University of Southern California, Los Angeles, California; and [5]Imaging Sciences Training Program, Radiology and Imaging Sciences, Clinical Center, National Institute of Biomedical Imaging and Bioengineering, National Institutes of Health, Bethesda, Maryland

Abraxane (nanoparticle albumin-bound paclitaxel) is an anticancer drug approved by the Food and Drug Administration. However, the mechanism of action of Abraxane is complex, and no established biomarker is available to accurately monitor its treatment outcomes. The aim of this study was to investigate whether the integrin-specific PET tracer ^{18}F-FPPRGD2 (investigational new drug 104150) can be used to monitor early response of tumors to Abraxane therapy. **Methods:** Orthotopic MDA-MB-435 breast cancer mice were treated with Abraxane (25 mg/kg every other day, 3 doses) or phosphate-buffered saline. Tumor volume was monitored by caliper measurement. PET scans were obtained before and at different times after the start of treatment (days 0, 3, 7, 14, and 21) using ^{18}F-FPPRGD2 and ^{18}F-FDG. The tumoricidal effect was also assessed ex vivo by immunohistochemistry. **Results:** Abraxane treatment inhibited the tumor growth, and a significant difference in tumor volume could be seen at day 5 after the initiation of treatment. The tumor uptake of ^{18}F-FPPRGD2 in the Abraxane-treated group was significantly lower on days 3 and 7 than at baseline but returned to the baseline level at days 14 and 21, indicative of relapse of the tumors after the treatment was halted. Immunohistologic staining confirmed that the change of ^{18}F-FPPRGD2 uptake correlated with the variation of integrin level in the tumor vasculature induced by Abraxane treatment. No significant change of tumor (rather than vascular) integrin expression was observed throughout the study. No significant decrease of ^{18}F-FDG uptake was found between the treated and the control tumors on days 3, 14, and 21, although an increase in ^{18}F-FDG tumor uptake of treated mice, as compared with the control mice, was found on day 7. The increase of ^{18}F-FDG on day 7 was related to the inflammatory response during therapy. **Conclusion:** Abraxane-mediated downregulation of integrin $\alpha_v\beta_3$ expression on tumor endothelial cells can be quantitatively visualized by PET. The change of integrin expression precedes that of tumor size. Consequently, ^{18}F-FPPRGD2 PET is superior to ^{18}F-FDG PET in monitoring early response to treatment, favoring its potential clinical translation.

Key Words: therapy response; positron emission tomography (PET); Abraxane; ^{18}F-FDG; RGD

J Nucl Med 2011; 52:140–146
DOI: 10.2967/jnumed.110.080606

Paclitaxel was originally derived from the bark of the Pacific Yew tree in the early 1960s. It can disrupt microtubule reorganization and lead to G2/M cell cycle arrest (*1*). As a potent cytotoxic agent, paclitaxel is widely used against various refractory and metastatic malignancies (*2,3*). However, it is also well known for its ability to produce hypersensitivity reactions and its limited aqueous solubility (*4,5*). The clinical use of paclitaxel has been improved significantly by formulating this drug in polyethoxylated castor oil–free, albumin-bound, 130-nm particles named Abraxane (nanoparticle albumin-bound paclitaxel; Abraxis BioScience).

Abraxane is an important therapeutic breakthrough, because it addresses the toxicities associated with solvents in taxane-based chemotherapy and minimizes the occurrence of severe anaphylactic reactions (*6,7*). In addition, compared with paclitaxel, Abraxane can improve drug delivery into the tumor (*8,9*). The antiangiogenesis activity of paclitaxel has been observed even at low concentrations, which did not affect cellular microtubule assembly (*10,11*). Paclitaxel also showed an inhibitory effect on the growth of transplanted human oral squamous cell carcinoma and reduced the expression of vascular endothelial growth factor (VEGF) and CD31 (*12*). However, contradictory reports also exist that Abraxane triggers reactionary angiogenesis by upregulating VEGF-A expression in a breast cancer model (*2*).

Integrins are composed of a family of heterodimeric glycoproteins responsible for the regulation of cellular

Received Jun. 25, 2010; revision accepted Sep. 17, 2010.

For correspondence or reprints contact either of the following: Xiaoyuan Chen, Laboratory of Molecular Imaging and Nanomedicine, National Institute of Biomedical Imaging and Bioengineering, National Institutes of Health, 31 Center Dr., 1C22, Bethesda, MD 20892-2281.
E-mail: shawn.chen@nih.gov
Gang Niu, Laboratory of Molecular Imaging and Nanomedicine, National Institute of Biomedical Imaging and Bioengineering, National Institutes of Health, 9 Memorial Dr., 9/1W111, Bethesda, MD 20892.
E-mail: niug@mail.nih.gov

activation, migration, proliferation, survival, and differentiation (*13*). One of the most important members of this receptor class is integrin $\alpha_v\beta_3$, which is preferentially expressed on several types of cancer cells, including melanoma, glioma, and ovarian and breast cancers (*14*). Integrin $\alpha_v\beta_3$ is also expressed on proliferating endothelial cells associated with neovascularization in both malignant tumors and normal tissue but not in quiescent blood vessels (*15,16*).

Because peptides containing arginine-glycine-aspartic acid (RGD) can bind strongly to integrin $\alpha_v\beta_3$, many RGD peptide probes have been developed for multimodality imaging of integrin expression (*17–21*). Targeting the $\alpha_v\beta_3$ integrin receptor could provide us with a tool to visualize and quantify integrin $\alpha_v\beta_3$ expression levels; early cellular and molecular effects of therapies (especially on vascular modulation), without having to rely on invasive histologic staining; consequential changes in blood perfusion and permeability; and terminal morphologic changes, such as substantial tumor mass or volume reduction (*14*).

^{18}F-FPPRGD2 is an ^{18}F-labeled dimeric RGD peptide recently developed in our laboratory that has higher receptor binding affinity than monomeric RGD peptide counterparts and enhanced tumor uptake (*22*). An exploratory investigative new drug application (IND 104150) for ^{18}F-FPPRGD2 was recently approved by the Food and Drug Administration for the first tests in humans. In this study, we performed longitudinal PET studies to compare the abilities of ^{18}F-FPPRGD2 and ^{18}F-FDG to evaluate the treatment efficacy of Abraxane in an MDA-MB-435 human breast cancer xenograft model.

MATERIALS AND METHODS

Radiochemistry

^{18}F-FPPRGD2 was synthesized as previously reported (*22*). In brief, PEG3-E[c(RGDyK)]$_2$ (denoted as PRGD2) was added to dried 4-nitrophenyl 2-^{18}F-fluoropropionate, followed by the addition of *N,N*-diisopropylethylamine. The labeled peptide was purified by reversed-phase high-performance liquid chromatography on a semipreparative C-18 column. After trapping with a C-18 cartridge preactivated with 5 mL of ethanol and 10 mL of water, the product was washed with 2 mL of water and eluted with 2 mL of ethanol. After the ethanol solution was blown dry with a slow stream of N_2 at 60°C, the ^{18}F-labeled peptide was redissolved in phosphate-buffered saline (PBS) solution and passed through a 0.22-μm Millipore filter into a sterile multidose vial for in vivo experiments. Radiochemical yield was approximately 95%. The specific activity was approximately 37 TBq/mmol.

Preparation of MDA-MB-435 Breast Cancer Model

The MDA-MB-435 human breast carcinoma tumor model known to express medium levels of integrin $\alpha_v\beta_3$ (*23*) was used for the in vivo imaging studies. The MDA-MB-435 cell line was purchased from American Type Culture Collection and grown in Leibovitz's L-15 medium supplemented with 10% (v/v) fetal bovine serum under a 100% air atmosphere at 37°C. The MDA-MB-435 tumor model was generated by orthotopic injection of 5×10^6 cells in the left mammary fat pad of female athymic nude mice (Harlan Laboratories). The mice were used for studies when the tumor volume reached about 250 mm^3 (~10–14 d after implantation). Tumor growth was followed by caliper measurements of perpendicular diameters of the tumor. The tumor volume was estimated by the formula tumor volume = $a \times (b^2)/2$, where a and b were the tumor length and width, respectively, in millimeters. All animal experiments were performed in compliance with the guidelines for the care and use of research animals established by Stanford University's Animal Studies Committee.

Longitudinal Small-Animal PET Scans

PET scans and image analysis were performed using an Inveon microPET scanner (Siemens Medical Solutions). Each MDA-MB-435 tumor–bearing mouse was injected via the tail vein with 3.7 MBq (100 μCi) of ^{18}F-FPPRGD2 or 7.4 MBq (200 μCi) of ^{18}F-FDG under isoflurane anesthesia. Five-minute static scans were acquired at 1 h after injection. For the ^{18}F-FDG scan, mice were maintained under isoflurane anesthesia during the injection, accumulation, and scanning periods and were kept fasting for 4 h before tracer injection. For the ^{18}F-FPPRGD2 scan, mice were not anesthetized during the tracer accumulation period and were not kept fasting before tracer injection. The images were reconstructed and quantified using procedures described in the supplemental materials (supplemental materials are available online only at http://jnm.snmjournals.org).

As shown in Table 1, 40 mice underwent baseline PET with ^{18}F-FPPRGD2 (n = 20) or ^{18}F-FDG (n = 20) (day 0) when the tumors reached a size of around 250 mm^3. Then the tumor-bearing mice were randomly divided into the following 4 groups (n = 10/group): ^{18}F-FPPRGD2 control, ^{18}F-FPPRGD2 treatment, ^{18}F-FDG control, and ^{18}F-FDG treatment. Mice in the treatment groups received 3 doses of Abraxane diluted in PBS, and control mice received PBS only. Doses of Abraxane (25 mg/kg) or PBS were administered on days 0, 2, and 4. PET scans were repeated on days 3, 7, 14, and 21. At each time point, 1 mouse from each group was sacrificed, and the tumors were excised for histopathology.

Fluorescence Staining

Frozen tumor tissue slices (8 μm) were fixed with cold acetone for 20 min and dried in the air for 30 min at room temperature. After blocking with 1% bovine serum albumin for 30 min, the sections were incubated with humanized antihuman integrin $\alpha_v\beta_3$ antibody Abegrin (*24*) (20 μg/mL) for 1 h at room temperature and

TABLE 1
Experimental Design for Longitudinal ^{18}F-FDG and ^{18}F-FPPRGD2 Imaging of Abraxane Treatment Efficacy and Ex Vivo Histopathology

Parameter	Day 0	2	3	4	7	14	21
^{18}F-FPPRGD2	#, +	+	#	+	#	#	#
Control							
Abraxane	#, +	+	#	+	#	#	#
^{18}F-FDG							
Control	#, +	+	#	+	#	#	#
Abraxane	#, +	+	#	+	#	#	#
Histology	–		–		–		–

= small-animal PET; + = PBS or Abraxane treatment; – = tumor tissue sampling.

then visualized with cy3-conjugated donkey antihuman secondary antibodies (1:300; Jackson ImmunoResearch Laboratories). For the overlay staining of CD31 and CD61, slices were incubated with rat antimouse CD31 antibody (1:200; BD Biosciences) and hamster anti-β3 CD61 antibody (1:200; BD Biosciences) and then visualized with cy3-conjugated goat antirat and fluorescein isothiocyanate–conjugated goat antihamster secondary antibody (1:300; Jackson ImmunoResearch Laboratories). For the overlay staining of Ki67 and F4/80, slices were incubated with rabbit antimouse Ki76 antibody (1:200; BD Biosciences) and rat antimouse F4/80 antibody (1:200; Abcam, Inc.) and then visualized with cy3-conjugated goat antirabbit and fluorescein isothiocyanate–conjugated goat antirat secondary antibody (1:300; Jackson ImmunoResearch Laboratories). After being washed 5 times with PBS, the slices were mounted with 4′-6-diamidino-2-phenylindole (DAPI)-containing mounting medium and observed under an epifluorescence microscope (X81; Olympus). Each experiment was performed in pairs, and the pairs were then repeated twice.

Statistical Analysis

Quantitative data were expressed as means ± SD. Means were compared using 1-way ANOVA and a Student *t* test. *P* values less than 0.05 were considered statistically significant. Unpaired Student *t* tests were used to evaluate differences between the 2 treatment groups, and paired Student *t* tests were performed for differences between time points on the activity curve within a treatment condition.

RESULTS

Abraxane Treatment–Inhibited MDA-MB-435 Tumor Growth

Abraxane is effective in delaying MDA-MB-435 tumor growth. Intravenous administration of 3 doses of Abraxane (25 mg/kg; days 0, 2, and 4) resulted in a reduction in tumor volume. As shown in Figure 1A, a time-related increase in tumor volume was observed in the PBS control group, in which the tumors showed an average fractional tumor volume (V/V_0) of 1.27, 1.42, 1.51, 1.78, and 2.63 on days 3, 5, 7, 14, and 21, respectively. Abraxane treatment resulted in a V/V_0 of 0.99, 0.78, 0.67, 0.51, and 0.65 on days 3, 5, 7, 14, and 21, respectively. The average tumor size of the control group became significantly smaller than that of the treatment group starting from day 5 ($P < 0.05$). In the treated mice, an increase of fractional tumor volume from day 14 ($V/V_0 = 0.51$) to day 21 ($V/V_0 = 0.65$) was noted. This pattern of initial response during and immediately after the treatment, and then regrowth after the treatment was stopped, is common in many other experimental cancer therapy studies and clinical cancer trials (*25–27*). Mouse body weight was monitored as an indicator of the toxicity of Abraxane. As evidenced in Figure 1B, it is clear that Abraxane had no observable side effects at the low dosage used in this study.

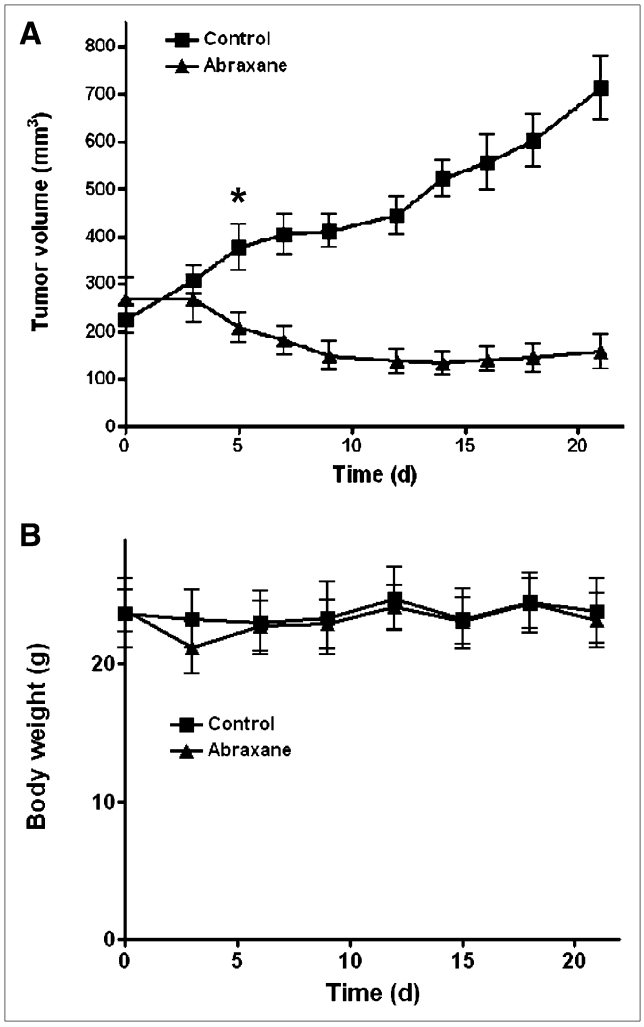

FIGURE 1. Antitumor activity of Abraxane in established MDA-MB-435 xenografts. (A) 3 doses of Abraxane (intravenous injection, 25 mg/kg/dose on days 0, 2, and 4) led to substantial tumor regression but also regrowth after day 14. (B) Body weight of animals treated with PBS or Abraxane.

PET with ^{18}F-FPPRGD2 and ^{18}F-FDG

Static PET images at 1 h after injection of ^{18}F-FDG (Fig. 2) or ^{18}F-FPPRGD2 (Fig. 3) were acquired at day 0 (baseline, before Abraxane treatment) and at days 3, 7, 14, and 21 after the Abraxane treatment was initiated. The tumor region-of-interest analysis is summarized in Figure 4. As shown in Figures 2 and 4A, there was little fluctuation of ^{18}F-FDG uptake in the control mice at different days after tumor inoculation. Abraxane treatment led to some increase of ^{18}F-FDG uptake at days 3 and 7, which returned to the baseline level at days 14 and 21. Figures 3 and 4B describe the tumor uptake pattern of ^{18}F-FPPRGD2 with and without Abraxane treatment. After Abraxane treatment, the MDA-MB-435 tumor uptake of ^{18}F-FPPRGD2 significantly decreased from 1.22 ± 0.08 percentage injected dose per gram (%ID/g) (day 0) to 1.08 ± 0.10 %ID/g (day 3, $P < 0.05$) and 0.63 ± 0.06 %ID/g (day 7, $P < 0.01$), which represents a decrease of up to 48%. At days 14 and 21, the ^{18}F-FPPRGD2 in the treated mice increased to the level in the control mice, with tumor uptake of 1.42 ± 0.14 and 1.23 ± 0.19 %ID/g, respectively.

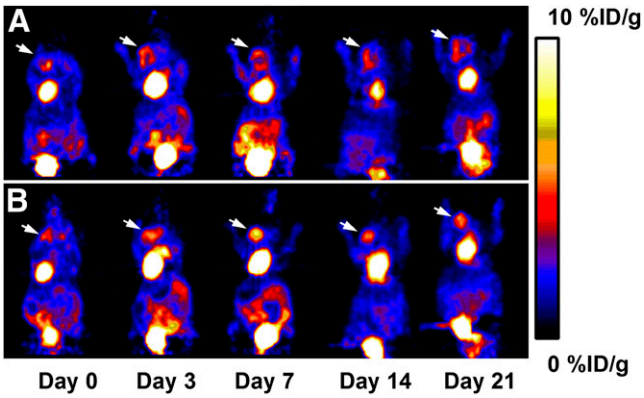

FIGURE 2. Representative decay-corrected whole-body coronal images of female athymic nude mice bearing orthotopic MDA-MB-435 tumors at 1 h after intravenous injection of ^{18}F-FDG (7.4 MBq/mouse) on days 0, 3, 7, 14, and 21 after treatment was initiated. Increased uptake of ^{18}F-FDG was observed on days 3 and 7, decreasing to baseline level on days 14 and 21. (A) PBS control. (B) Abraxane treatment.

Abraxane-Induced Inflammation and Inhibition of Proliferation

To evaluate the therapeutic effect of Abraxane on MDA-MB-435 tumors, we performed Ki67 immunofluorescence staining on tumor sections. The percentage of Ki67-positive cells (Ki67 staining index) in untreated tumors was around 72% ± 17%, independent of the tumor size (Fig. 5). Consistent with the tumor growth inhibition, significantly delayed cell proliferation was observed in the Abraxane-treated mice at days 3 and 7 with a Ki67 SI of 17% ± 7% and 22% ± 5%, respectively ($P < 0.01$) (Supplemental Fig. 1). The Ki67 SI was restored to the baseline level at days 14 and 21.

The tumor sections were also stained against macrophage-specific marker F4/80 to evaluate Abraxane-induced inflammation. Compared with control tumors, a more pronounced inflammatory reaction was observed at days 3 and 7 after treatment. At day 14, F4/80-positive macrophages decreased significantly ($P < 0.01$) (Supplemental Fig. 2).

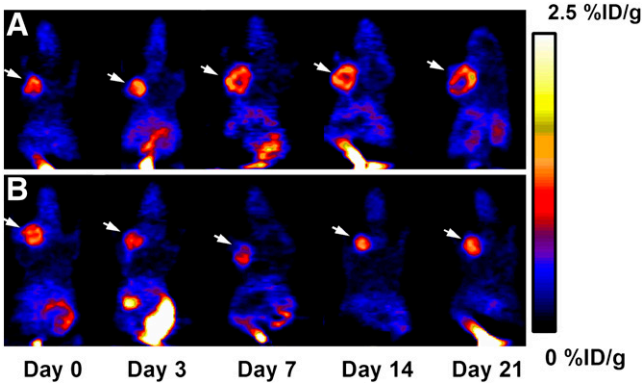

FIGURE 3. Representative decay-corrected whole-body coronal images of female athymic nude mice bearing orthotopic MDA-MB-435 tumors at 1 h after intravenous injection of ^{18}F-FPPRGD2 (3.7 MBq/mouse) on days 0, 3, 7, 14, and 21 after treatment was initiated. Decreased tumor uptake of ^{18}F-FPPRGD2 was observed on days 3 and 7 but was restored to baseline level on days 14 and 21. (A) PBS control. (B) Abraxane treatment.

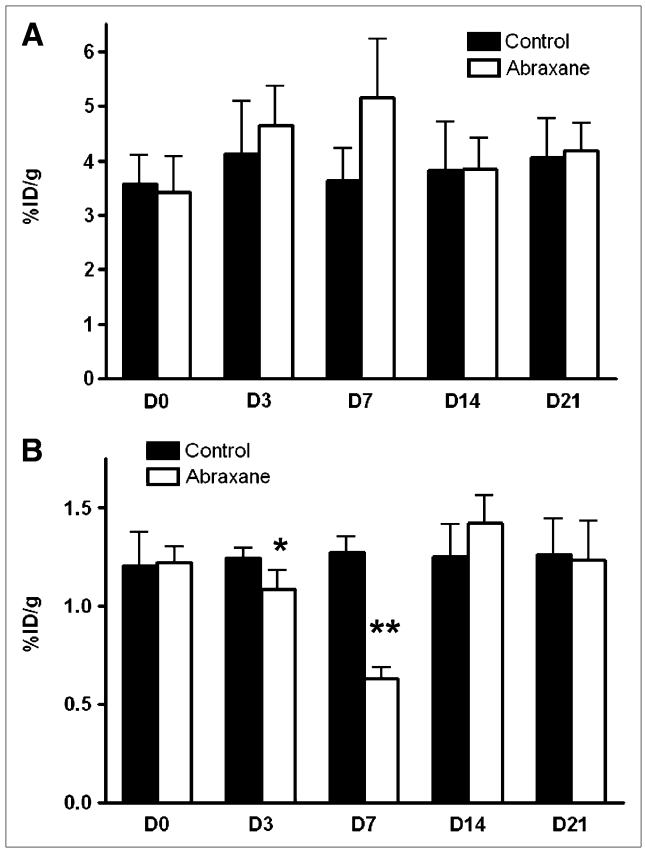

FIGURE 4. Quantitative small-animal PET region-of-interest analysis of tumor uptake for ^{18}F-FDG (A) and ^{18}F-FPPRGD2 (B).

Effect of Abraxane on Tumor Integrin Expression

To further investigate the mechanism of altered ^{18}F-FPPRGD2 uptake during and after Abraxane treatment, integrin expression was evaluated by immunofluorescence staining. Because integrin on tumor vascular endothelial cells was of murine origin and that on tumor cells was of human origin, we stained tumor sections with both antimurine integrin β3 and antihuman integrin $\alpha_v\beta_3$ antibodies. As shown in Figure 6A, MDA-MB-435 tumor cells had positive human integrin $\alpha_v\beta_3$ staining, which was unaffected by Abraxane treatment.

Murine β3 was colocalized with murine CD31, indicating that the expression of murine integrin β3 was mainly on the tumor vascular endothelial cells. A significant morphologic change of tumor vasculature, including the collapse of microvessel cavities, was observed in Abraxane-treated tumors at different times. In addition, after Image J (National Institutes of Health) analysis, we found that the mean murine β3 fluorescence intensity decreased significantly at days 3 ($P < 0.05$) and 7 ($P < 0.01$) (Supplemental Fig. 3) after Abraxane treatment; the treated tumors and control tumors had similar vascular integrin levels at days 14 and 21, correlating with the ^{18}F-FPPRGD2 imaging studies.

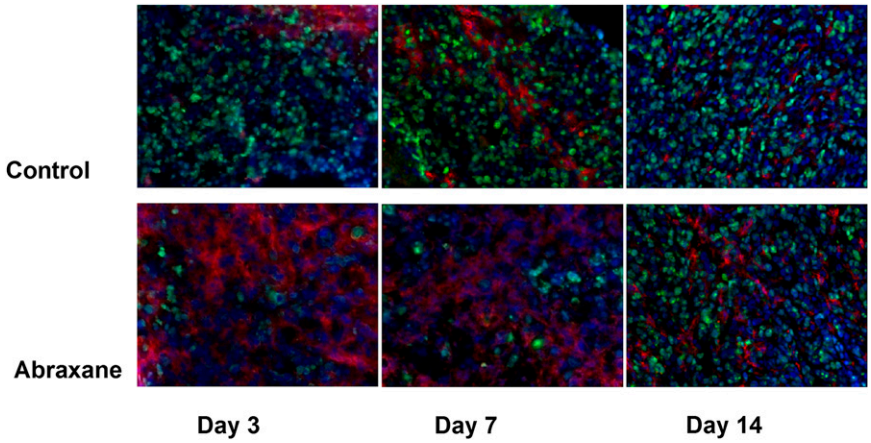

FIGURE 5. Ex vivo overlay staining of tumor sections from PBS- and Abraxane-treated MDA-MB-435 tumors on days 3, 7, and 14. Green = Ki67; red = F4/80; blue = DAPI.

DISCUSSION

The ability to visualize and quantify integrin $\alpha_v\beta_3$ expression levels noninvasively in vivo provides new opportunities to document integrin expression, greatly assist the understanding of mechanisms of angiogenesis and antiangiogenic treatment, and monitor treatment efficacy. We have previously reported a series of radiolabeled RGD monomers and multimers for imaging integrin $\alpha_v\beta_3$ expression (*18,22,28–32*). Among them, ^{18}F-FPPRGD2, with relatively high tumor integrin-specific accumulation and favorable in vivo kinetics, has made its way into the clinic for cancer diagnosis and for treatment response monitoring (*22*).

There have been several studies using suitably labeled monomeric RGD peptide tracers to monitor chemotherapy or antiangiogenic treatment efficacy. For example, paclitaxel therapy in Lewis lung carcinoma tumor–bearing mice significantly retarded tumor growth and was accompanied by a corresponding reduction of tumor glucosamino ^{99m}Tc-D-c(RGDfK) uptake, as determined by γ-camera imaging,

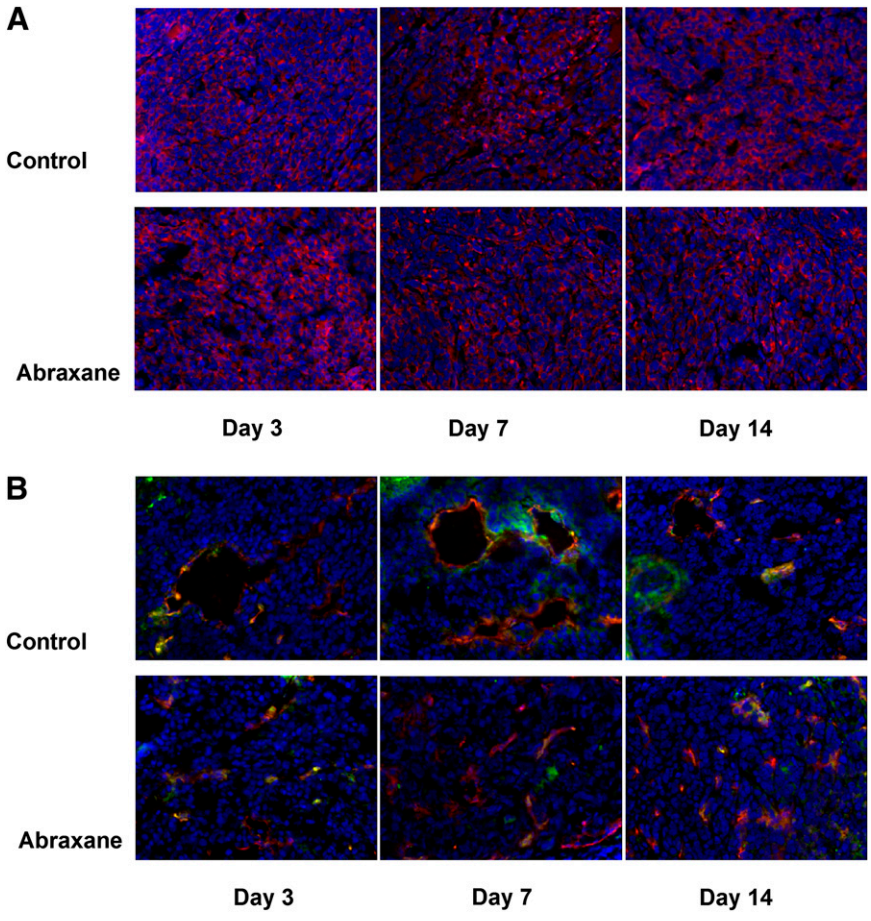

FIGURE 6. (A) Ex vivo human integrin staining of tumor sections from PBS- and Abraxane-treated MDA-MB-435 tumors on days 3, 7, and 14. (B) Overlay staining of CD31 (red), murine integrin β3 (green), and DAPI (blue) of tumor sections from PBS- and Abraxane-treated MDA-MB-435 tumors on days 3, 7, and 14.

correlating well with tumor α_v integrin expression levels (*33*). Similarly, paclitaxel therapy reduced the microvessel density in Lewis lung carcinoma tumor–bearing mice and resulted in significantly reduced tumor uptake of ^{18}F-AH111585. ZD4190 (a small-molecular-weight VEGF receptor-2 tyrosine kinase inhibitor) therapy resulted in a significant decrease in ^{18}F-AH111585 uptake in Calu-6 tumors, compared with vehicle control-treated Calu-6 tumors (*34*). Dasatinib, an Src-family kinase inhibitor, reduced ^{64}Cu-DOTA-c(RGDfK) uptake in a U87MG xenograft model. In contrast, tumor ^{18}F-FDG uptake showed no significant reduction with dasatinib therapy (*35*). All these studies supported the feasibility of noninvasive imaging using RGD-based probes to monitor antiangiogenic therapy response.

In this study, we investigated the potential of ^{18}F-FPPRGD2 to accurately assess therapeutic response of human mammary carcinomas to Abraxane treatment and to be translated into the clinic for integrin $\alpha_v\beta_3$ imaging. In vivo small-animal PET showed that there was a significant reduction in the tumor uptake of ^{18}F-FFPPRGD2 as early as day 3 after the initiation of Abraxane treatment. Moreover, this reduction in tumor accumulation of ^{18}F-FPPRGD2 was observed before a tumor size decrease could be discerned by caliper measurement, suggesting that ^{18}F-FPPRGD2 can detect early responses preceding clinical regression. We also performed a comparison study with ^{18}F-FDG as an imaging tracer. ^{18}F-FDG showed increased tumor uptake at days 3 and 7, despite positive tumor response to Abraxane treatment.

It is worth mentioning that our longitudinal scans showed an initial decrease and subsequent restoration of ^{18}F-FPPRGD2 after Abraxane treatment, as is consistent with the pattern of initial growth inhibition and tumor relapse after treatment is stopped. However, the change of ^{18}F-FPPRGD2 uptake accurately predicted the tumor response a few days before the anatomic tumor size change could be accurately measured. Immunohistochemical staining also confirmed that the change of ^{18}F-FPPRGD2 uptake reflected tumor vascular integrin level, rather than tumor cell integrin expression (which was unaffected by Abraxane treatment). The exact mechanism by which Abraxane affects the vascular integrin but not tumor cell integrin expression is not well understood and will be a subject of future studies.

Despite the cytoxicity of Abraxane, ^{18}F-FDG uptake was somewhat increased at the early stage of treatment, possibly because of the combined effect of reduced tumor cell proliferation (Ki67 index) and increased macrophage infiltration (F4/80 staining) in regressing tumors. It has been well documented that ^{18}F-FDG can show high uptake when inflammatory cells are present (*36,37*)—which is the potential limitation of ^{18}F-FDG when used to monitor therapeutic response. ^{18}F-FPPRGD2 is superior to ^{18}F-FDG, because the uptake of ^{18}F-FPPRGD2 seems not to be influenced by tumor-associated macrophages after therapy. Thus, it can identify MDA-MB-435 tumor response to Abraxane more accurately.

The promising imaging results elucidated in this longitudinal study suggest the usefulness of quantitative ^{18}F-FPPRGD2 PET to evaluate treatments that produce an antiangiogenic effect and a change in vascular integrin level. However, we have to bear in mind that tumor uptake and accumulation of a given radiotracer are not solely dependent on receptor expression. Several other factors, including vascular density and volume, vascular permeability, and interstitial fluid pressure, also affect the distribution (*38,39*). To explore the usefulness of ^{18}F-FPPRGD2 in monitoring treatment response, studies in various tumor models with different integrin $\alpha_v\beta_3$ expression patterns and different sensitivities to certain therapeutics should be conducted. In certain cases, receptor binding potential derived from dynamic scans, instead of tumor uptake or tumor-to-background ratio, might be needed to eliminate the influence of tumor microenvironment on the pharmacokinetics of ^{18}F-FPPRGD2. ^{18}F-FPPRGD2 alone or in combination with additional functional imaging modalities can enhance our mechanistic understanding of how novel molecular therapeutic strategies affect tumors and allow early prediction of treatment efficacy and potential relapse, leading to better individualization of chemotherapy.

CONCLUSION

Our data illustrate that ^{18}F-FPPRGD2 is a promising PET tracer that allows noninvasive evaluation of response to treatments that affect integrin $\alpha_v\beta_3$ level, before size changes can be found. It also has the potential to provide earlier clinical opportunities to adjust anticancer drug doses and intervals to maintain sustained antitumor effect and avoid relapse. ^{18}F-FPPRGD2 is superior to ^{18}F-FDG in monitoring anticancer treatment, because ^{18}F-FPPRGD2 imaging is not significantly affected by the presence of infiltrating macrophages in regressing tumors.

ACKNOWLEDGMENTS

We thank Dr. Henry S. Eden for proofreading this manuscript. This project was supported by the Intramural Research Program of the National Institute of Biomedical Imaging and Bioengineering (NIBIB), National Institutes of Health (NIH); the Radiology and Imaging Sciences Department, NIH Clinical Center; and the Intramural Research Program, NIBIB, NIH.

REFERENCES

1. Li CJ, Li YZ, Pinto AV, Pardee AB. Potent inhibition of tumor survival in vivo by beta-lapachone plus taxol: combining drugs imposes different artificial checkpoints. *Proc Natl Acad Sci USA.* 1999;96:13369–13374.
2. Volk LD, Flister MJ, Bivens CM, et al. Nab-paclitaxel efficacy in the orthotopic model of human breast cancer is significantly enhanced by concurrent anti-vascular endothelial growth factor A therapy. *Neoplasia.* 2008;10:613–623.
3. Damascelli B, Cantu G, Mattavelli F, et al. Intraarterial chemotherapy with polyoxyethylated castor oil free paclitaxel, incorporated in albumin nanoparticles (ABI-007): phase II study of patients with squamous cell carcinoma of the head and neck and anal canal—preliminary evidence of clinical activity. *Cancer.* 2001;92:2592–2602.
4. Rodriguez-Antona C. Pharmacogenomics of paclitaxel. *Pharmacogenomics.* 2010;11:621–623.

5. Singh S, Dash AK. Paclitaxel in cancer treatment: perspectives and prospects of its delivery challenges. *Crit Rev Ther Drug Carrier Syst.* 2009;26:333–372.
6. Desai N, Trieu V, Yao Z, et al. Increased antitumor activity, intratumor paclitaxel concentrations, and endothelial cell transport of cremophor-free, albumin-bound paclitaxel, ABI-007, compared with cremophor-based paclitaxel. *Clin Cancer Res.* 2006;12:1317–1324.
7. Gradishar WJ, Tjulandin S, Davidson N, et al. Phase III trial of nanoparticle albumin-bound paclitaxel compared with polyethylated castor oil-based paclitaxel in women with breast cancer. *J Clin Oncol.* 2005;23:7794–7803.
8. Petrelli F, Borgonovo K, Barni S. Targeted delivery for breast cancer therapy: the history of nanoparticle-albumin-bound paclitaxel. *Expert Opin Pharmacother.* 2010;11:1413–1432.
9. Link JS, Waisman JR, Nguyen B, Jacobs CI. Bevacizumab and albumin-bound paclitaxel treatment in metastatic breast cancer. *Clin Breast Cancer.* 2007;7: 779–783.
10. Belotti D, Vergani V, Drudis T, et al. The microtubule-affecting drug paclitaxel has antiangiogenic activity. *Clin Cancer Res.* 1996;2:1843–1849.
11. Wang J, Lou P, Lesniewski R, Henkin J. Paclitaxel at ultra low concentrations inhibits angiogenesis without affecting cellular microtubule assembly. *Anticancer Drugs.* 2003;14:13–19.
12. Myoung H, Hong SD, Kim YY, Hong SP, Kim MJ. Evaluation of the anti-tumor and anti-angiogenic effect of paclitaxel and thalidomide on the xenotransplanted oral squamous cell carcinoma. *Cancer Lett.* 2001;163:191–200.
13. Ruegg C, Alghisi GC. Vascular integrins: therapeutic and imaging targets of tumor angiogenesis. *Recent Results Cancer Res.* 2010;180:83–101.
14. Desgrosellier JS, Cheresh DA. Integrins in cancer: biological implications and therapeutic opportunities. *Nat Rev Cancer.* 2010;10:9–22.
15. Kassmeyer S, Plendl J, Custodis P, Bahramsoltani M. New insights in vascular development: vasculogenesis and endothelial progenitor cells. *Anat Histol Embryol.* 2009;38:1–11.
16. Weis SM. Evaluating integrin function in models of angiogenesis and vascular permeability. *Methods Enzymol.* 2007;426:505–528.
17. Cai W, Chen X. Multimodality molecular imaging of tumor angiogenesis. *J Nucl Med.* 2008;49(suppl 2):113S–128S.
18. Chen X. Multimodality imaging of tumor integrin αvβ3 expression. *Mini Rev Med Chem.* 2006;6:227–234.
19. Liu Z, Li ZB, Cao Q, Liu S, Wang F, Chen X. Small-animal PET of tumors with ^{64}Cu-labeled RGD-bombesin heterodimer. *J Nucl Med.* 2009;50:1168–1177.
20. Dimastromatteo J, Riou LM, Ahmadi M, et al. In vivo molecular imaging of myocardial angiogenesis using the αvβ3 integrin-targeted tracer ^{99m}Tc-RAFT-RGD. *J Nucl Cardiol.* 2010;17:435–443.
21. Myers TA, Kaushal D, Philipp MT. Microglia are mediators of Borrelia burgdorferi-induced apoptosis in SH-SY5Y neuronal cells. *PLoS Pathog.* 2009;5: e1000659.
22. Liu S, Liu Z, Chen K, et al. ^{18}F-labeled galacto and PEGylated RGD dimers for PET imaging of αvβ3 integrin expression. *Mol Imaging Biol.* 2010;12: 530–538.
23. Zhang X, Xiong Z, Wu Y, et al. Quantitative PET imaging of tumor integrin αvβ3 expression with ^{18}F-FRGD2. *J Nucl Med.* 2006;47:113–121.
24. Liu Z, Jia B, Zhao H, Chen X, Wang F. Specific targeting of human integrin αvβ3 with ^{111}In-labeled abegrin in nude mouse models. *Mol Imaging Biol.* April 10, 2010 [Epub ahead of print].
25. Cao Q, Li ZB, Chen K, et al. Evaluation of biodistribution and anti-tumor effect of a dimeric RGD peptide-paclitaxel conjugate in mice with breast cancer. *Eur J Nucl Med Mol Imaging.* 2008;35:1489–1498.
26. Wang H, Chen K, Cai W, et al. Integrin-targeted imaging and therapy with RGD4C-TNF fusion protein. *Mol Cancer Ther.* 2008;7:1044–1053.
27. Niu G, Chen X. Has molecular and cellular imaging enhanced drug discovery and drug development? *Drugs R D.* 2008;9:351–368.
28. Shi J, Kim YS, Zhai S, Liu Z, Chen X, Liu S. Improving tumor uptake and pharmacokinetics of ^{64}Cu-labeled cyclic RGD peptide dimers with Gly_3 and PEG_4 linkers. *Bioconjug Chem.* 2009;20:750–759.
29. Liu Z, Niu G, Shi J, Liu S, Wang F, Chen X. ^{68}Ga-labeled cyclic RGD dimers with Gly3 and PEG4 linkers: promising agents for tumor integrin αvβ3 PET imaging. *Eur J Nucl Med Mol Imaging.* 2009;36:947–957.
30. Li ZB, Cai W, Cao Q, et al. ^{64}Cu-labeled tetrameric and octameric RGD peptides for small-animal PET of tumor αvβ3 integrin expression. *J Nucl Med.* 2007;48:1162–1171.
31. Wu Z, Li ZB, Chen K, et al. microPET of tumor integrin αvβ3 expression using ^{18}F-labeled PEGylated tetrameric RGD peptide (^{18}F-FPRGD4). *J Nucl Med.* 2007;48:1536–1544.
32. Cai W, Niu G, Chen X. Imaging of integrins as biomarkers for tumor angiogenesis. *Curr Pharm Des.* 2008;14:2943–2973.
33. Jung KH, Lee KH, Paik JY, et al. Favorable biokinetic and tumor-targeting properties of ^{99m}Tc-labeled glucosamino RGD and effect of paclitaxel therapy. *J Nucl Med.* 2006;47:2000–2007.
34. Morrison MS, Ricketts SA, Barnett J, Cuthbertson A, Tessier J, Wedge SR. Use of a novel Arg-Gly-Asp radioligand, ^{18}F-AH111585, to determine changes in tumor vascularity after antitumor therapy. *J Nucl Med.* 2009;50:116–122.
35. Dumont RA, Hildebrandt I, Su H, et al. Noninvasive imaging of αvβ3 function as a predictor of the antimigratory and antiproliferative effects of dasatinib. *Cancer Res.* 2009;69:3173–3179.
36. Avril N, Menzel M, Dose J, et al. Glucose metabolism of breast cancer assessed by ^{18}F-FDG PET: histologic and immunohistochemical tissue analysis. *J Nucl Med.* 2001;42:9–16.
37. Kubota R, Yamada S, Kubota K, Ishiwata K, Tamahashi N, Ido T. Intratumoral distribution of fluorine-18-fluorodeoxyglucose in vivo: high accumulation in macrophages and granulation tissues studied by microautoradiography. *J Nucl Med.* 1992;33:1972–1980.
38. Niu G, Li Z, Xie J, Le QT, Chen X. PET of EGFR antibody distribution in head and neck squamous cell carcinoma models. *J Nucl Med.* 2009;50:1116–1123.
39. Niu G, Sun X, Cao Q, et al. Cetuximab-based immunotherapy and radioimmunotherapy of head and neck squamous cell carcinoma. *Clin Cancer Res.* 2010;16:2095–2105.